Classical field records of a quantum system: Their internal consistency and accuracy

Joanna Pietraszewicz and Piotr Deuar
Institute of Physics, Polish Academy of Sciences, Aleja Lotników 32/46, 02-668 Warsaw, Poland
(Received 28 April 2015; revised manuscript received 1 October 2015; published 10 December 2015)

We determine the regime where the widespread classical field description for quantum Bose gases is quantitatively accurate in one dimension (1D), 2D, and 3D by a careful study of the ideal gas limit. Numerical benchmarking in 1D shows that the ideal gas results carry over unchanged into the weakly interacting gas. The optimum high-energy cutoff is in general shown to depend strongly on the observable in question (e.g., energy, density fluctuations, phase coherence length, condensate fraction). This explains the wide range of past results. A consistent classical field representation with less than 10% deviation in all typical observables can be given for systems at temperatures below 0.0064 degeneracy temperature in 1D, and 0.49 critical temperature in 3D. Surprisingly, this is not possible for the two-dimensional ideal gas even at zero temperature because mean density, density fluctuations, and energy cannot be simultaneously matched to the quantum results.

DOI: 10.1103/PhysRevA.92.063620 PACS number(s): 03.75.Hh, 05.30.Jp, 67.85.Hj

I. INTRODUCTION

The quantum mechanics of a wide variety of physical systems can be quite accurately described by an appropriately chosen ensemble of complex fields (also called classical or c-fields) [1–5]. Examples include quantum gases of ultracold atoms, coherent light fields, and solid-state polariton systems. A common feature is the appearance of collective behavior such as high-amplitude phase fluctuations and superfluid defects, that strongly fluctuate away from the mean field. Though the term "classical" is used, we are talking about the opposite regime to the usual gas of classical particles. Here, it is the collective field that has classical properties such that each member of the ensemble could be nondestructively tracked, while the particles lose their individual identity. Examples of such approaches include classical field ensembles [1,3,6–8], the stochastic Gross-Pitaevski equation [2,9,10], the truncated Wigner representation [11–13] for ultracold atoms, and the open stochastic classical field equations for polaritons [14,15]. Related approaches for fermions include stochastic mean-field theory in, e.g., heavy-ion collisions [16,17], and effective field theories for the pairing order parameter [18,19].

In the absence of sufficient *in situ* experimental resolution, the approach is also commonly used like a flight recorder to give information on the dynamics of the system before its detection in destructive time-of-flight images. Its applications are growing in importance given advances in the experimental investigation of spontaneous superfluid defects and phase fluctuations, such as in Refs. [20–29]. In quantum many-body systems with collective nonlinear phenomena, such ensembles of complex fields are often the only practical way to obtain theoretical information on fluctuations, full distribution functions, and, especially, on typical single realizations with superfluid defects or quasicondensate phase fluctuations [8,28,30–46].

However, their use has usually been accompanied by lingering doubt on whether the results are quantitative or qualitative. From an operational perspective, two major contributing factors to that have been (i) a visible dependence of some results on the high-energy cutoff that is chosen, and (ii) different optimum cutoff values found in the literature [1,4,12,46–54]. The aim of this paper is to identify a regime where c-fields are in fact quantitatively accurate, so that they can be used there with confidence.

Qualitatively, the condition for the applicability of classical fields to bosons is that the relevant physics can be captured by considering only the highly occupied single-particle modes, without the need for a condensate [5]. Poorly occupied modes are not described well, and those above an energy cutoff need to be discarded to avoid pathological behavior, such as the UV catastrophe known since late 19th century physics.

However, the matter of just where to draw the line and how accurate the description is has been a matter of much contention and ambiguity. The history of applying classical fields to ultracold atomic gases teaches us that accuracy has depended quite strongly on the choice of the high-energy cutoff and the observables studied. Past numerical benchmarking [4,12,30,47–50,52,55–59], careful comparisons to experiment [48,60–62], and also analytical [50,51] and purely mathematical studies [63] of various single observables have found that it is possible to achieve good to very good agreement, but the details of the recipe vary from study to study [1,12,48,50,52].

Here, we intend to clarify these dependencies, and will show that under the right conditions the classical field approximation can be treated as more than just a qualitative guide, but gives predictions that are correct within small error bounds for a wide range of observables.

We will concentrate first on the case of an ideal gas as a baseline, reasoning that well-described interacting regimes can be found at temperatures that are already well described in the ideal gas. Then we will confirm that accuracy seen in the ideal gas carries over into the weakly interacting regime under appropriate conditions. We will work in the local density approximation (LDA) in the thermodynamic limit. That is, we will consider pieces of the gas cloud having a certain local density, which allows us to remain general in terms of trap geometry. In the LDA, it is natural to work in the grand canonical ensemble (GCE), where the rest of the system acts as the particle and thermal reservoir. Such a model underpins more general behavior, and it will be seen that several important conclusions can be reached.

In Sec. II we will describe our approach. Further, in Sec. III A, we will find the temperature-dependent eigencutoffs that allow the classical fields to correctly match the density and one other observable. Subsequently, in Secs. III B and IV we will determine the resulting errors in other observables and the cutoff that minimizes the systematic error across the whole range of observables. This will tell us about the temperature range over which an accurate complex field description of the system is possible. Finally, via numerical benchmarking of a weakly interacting gas in one dimension (1D) to the exact Yang and Yang solution [64] we will show in Sec. VI that the ideal gas results carry over largely unchanged into that regime. We conclude in Sec. VII.

II. APPROACH

A. Classical field description

The essence of the classical fields method is to replace annihilation (creation) operators $\hat{a}_k$ ($\hat{a}_k^\dagger$) of single-particle modes in the field operator by complex amplitudes ξ_k (ξ_k^*), which is warranted when occupation is macroscopic. Then we can write:

$$\hat{\Psi}(\mathbf{x}) = \sum_k \hat{a}_k \psi_k(\mathbf{x}) \to \left\{ \sum_{k\in\mathcal{C}} \xi_k \psi_k(\mathbf{x}) \right\}, \tag{1}$$

where $\psi_k(\mathbf{x})$ is the wave function for the kth mode and $\mathcal{C}$ denotes the low-energy subspace. Since we will be considering uniform sections of the gas, plane wave modes $k \equiv \mathbf{k}$ are the most convenient, with momentum cutoff k_c so that only modes $|\mathbf{k}| < k_c$ are included in $\mathcal{C}$.

In general, it should be understood that $\hat{\Psi}(\mathbf{x})$ corresponds to an ensemble $\{\ldots\}$ of complex field realizations, each with its own set of amplitudes ξ_k. The full ensemble preserves the gauge symmetry of the quantum thermal state that corresponds to a set of many experimental realizations. This is despite the virtual symmetry breaking done by each member of the ensemble similarly to a single experimental realization [5].

B. Parameters

The properties of the uniform dilute gas can be encapsulated by two dimensionless parameters. The first is $\gamma = \frac{mg}{\hbar^2 n}$ with density n and contact interaction strength g, and the second is a reduced temperature τ, which depends on the density n, but not on the interaction strength. We choose the thermal de Broglie wavelength $\Lambda_T = \sqrt{\frac{2\pi\hbar^2}{mk_BT}}$ as our length scale, so that the reduced temperature is

$$\tau = \frac{T}{T_d} = \frac{1}{2\pi}\frac{mk_B}{\hbar^2}\frac{T}{n^{2/d}}. \tag{2}$$

Here, T_d is the usual quantum degeneracy temperature in d dimensions that corresponds to one particle per region of volume Λ_T^d. It is a natural scale for our investigation because then $\tau = 1$ corresponds to the point at which the highest mode occupation is $O(1)$, and this constitutes the intuitive ultimate upper bound on temperature for which classical field descriptions make sense.

It is convenient to also scale the cutoff in these units:

$$f_c = k_c \frac{\Lambda_T}{2\pi}. \tag{3}$$

A value of $f_c = 1$ corresponds to a cutoff at the plane waves with thermal de Broglie wavelength Λ_T. We will henceforth work in the following units: $\Lambda_T = 1$ and $\hbar = m = 1$, where m is the mass of particles. Note that the cutoff in terms of single-particle energy is

$$\varepsilon_c = \pi\, k_B T\, f_c^2. \tag{4}$$

In the ideal gas limit ($\gamma \to 0$) that we consider first, there is only one physical parameter characterizing the system, the density-dependent reduced temperature τ, and one technical parameter f_c for the classical fields description. Phase space density equal to one occurs at $\tau = \tau_D = \{1.539, 1.443, 1.368\}$ in 1D, 2D, and 3D respectively, while the BEC critical temperature in 3D is $\tau = \tau_C = 0.5272$.

C. Observables

The great majority of experiments concentrate on low order observables such as phase, density or their fluctuations. We will analyze the following.

(i) n: density.

(ii) ε: kinetic energy per particle.

(iii) l_{pg}: phase grain length.

This is the size of a coherent region, which we will calculate via $l_{pg} := \frac{1}{n}\int d\mathbf{z}\, \langle\hat{\Psi}^\dagger(0)\hat{\Psi}(\mathbf{z})\rangle = \int d\mathbf{z}\, g^{(1)}(\mathbf{z})$. In the quasicondensate regime, when $g^{(1)}(\mathbf{z}) \simeq e^{-|\mathbf{z}|/l_\phi}$, l_{pg} equals the phase coherence length l_ϕ.

(iv) $g^{(2)}(0)$: normalized local density fluctuations.

While these are of much theoretical interest, they are rarely measured *in situ* because imaging resolution is usually much worse than the intrinsic density correlation length of the system.

(v) u_G: coarse-grained density fluctuations.

This quantity is defined as $u_G := \mathrm{var}N/\langle N\rangle = n\int d\mathbf{z}\,[g^{(2)}(\mathbf{z}) - 1] + 1$, where N is the atom number in a region much larger than the density correlation length. In contrast to $g^{(2)}(0)$, this intensive thermodynamic quantity often appears in experimental work [65,66] and it gives the ratio of the measured fluctuations in a pixel to Poisson shot noise. It is equal to the static structure factor at $|\mathbf{k}| = 0$, i.e., $S(0)$.

(vi) ρ_o: condensate fraction.

(vii) a_r: coherence half width.

In the presence of a true condensate, l_{pg} (and u_G) ceases to be a good thermodynamic quantity, diverging because $g^{(1)}(z \to \infty) = \rho_o$. In light of this we need another measure of the width of phase fluctuations, and will define it by the half width of the peak of $g^{(1)}(z)$, i.e., $g^{(1)}(a_r) = \frac{1}{2}(1 + \rho_o)$.

It is worth noting that the kinetic energy per particle in itself is not a typical subject of measurement, but its consideration has here its own justifications. If typical observable quantities are described correctly, but ϵ is not, then this will quickly come out as errors in the dynamics.

D. Ensemble

A major consideration in our work here has been to remain independent of trap geometry. This basically requires working in the local density approximation (LDA). As an example of variations with geometry that can occur without an LDA approach, optimal energy cutoffs found on the basis of the distribution of condensate fraction for a whole cloud in the canonical ensemble were $0.29k_BT$ in a uniform box, but $1.0k_BT$ for a harmonically trapped gas [50]. In the end in Sec. V A, we will see that the results of the LDA approach can be largely reconciled with the harmonically trapped canonical ensemble results.

When considering a relatively uniform section of a larger gas, it is not only possible, but also essential to work in the grand canonical ensemble (GCE) rather than the canonical one. In such a situation the rest of the system acts as a particle and thermal reservoir, while the uniform GCE section describes the properties that are local to the region. This approximation is acceptable provided the physical length scales such as l_{pg} are shorter than the length scale on which the density changes. Such conditions generally prevail for quasicondensates or a three-dimensional gas above the condensation temperature.

Use of the GCE in a truly condensed system such as the three-dimensional gas below T_c or the finite-size two-dimensional gas at extreme low temperatures, requires some care and background to get our bearings. It is known that for the ideal gas the usual thermodynamic equivalence between ensembles is lost in the presence of condensation. Particularly glaring differences are seen in the fluctuations of condensate fraction between the canonical and grand canonical ensemble—a matter that has been much studied [67–74] and is sometimes known as the fluctuation catastrophe for the GCE. In fact, a uniform condensed system in the GCE has anomalous fluctuations of the number of condensed particles (i.e., their variance grows faster than the mean number), which implies that some quantities such as u_G diverge. Technically this signals the point of the breakdown of the theory [75–77], but in reality this kind of behavior cannot actually occur. Physically, the growth of diverging quantities is braked by other effects. Usually, the causes can be traced to either a breakdown of the thermodynamic limit due to finite-size effects, or a suppression of fluctuations due to interactions (see Ref. [78] for a detailed discussion).

The primary difference between the grand canonical and microcanonical or canonical treatments of an ideal condensed system has been pointed out quite early [71] by studying the ground-state number fluctuations. They are huge in the GCE [the occupation N_0 of the ground state is exponentially distributed $P(N_0) \sim e^{\mu N_0/T}$] but small in the other thermodynamical ensembles. In contrast, there is no such difference for excited level occupations. This suggests that the majority of observables are not pathological. Even the mean condensate fraction does not diverge nor break equivalence between ensembles, unlike its fluctuations. Hence, it is legitimate to benchmark classical fields in the GCE provided that we exclude from consideration those observables that are known to be deviant. In particular, when condensation is present neither condensate fraction ρ_o nor the main coherence decay described by a_r are pathological, so we will use these instead of u_G and l_{pg}.

The suppression of anomalous condensate fluctuations due to interactions can occur even at very weak interactions. This can be seen from a simple argument: Consider the GCE partition function of the condensate mode:

$$Z_0(\mu,T) = \sum_{N_0=0}^{\infty} e^{(\mu N_0 - C_0 g N_0^2)/T} \tag{5}$$

with g the interaction strength, and C_0 a geometry-dependent factor [71]. In this form it is now a Gaussian distribution of the condensate occupation with mean $\overline{N}_0 = \mu/2gC_0$ and relative condensate number fluctuations $\Delta N_0/N_0 = \sqrt{T/(2C_0 g N_0^2)} = \sqrt{T/(2E_{\rm int})}$. It means that the relative magnitude of the number fluctuations is related to the ratio of the temperature to the interaction energy of the entire system, $E_{\rm int}$. The latter very quickly suppresses the grand canonical fluctuation catastrophe as the size of the system becomes appreciable, leaving only a tiny low-temperature region at $T \lesssim 1/E_{\rm int}$ with anomalous fluctuations, that shrinks as $T \to 0$.

The above considerations are distinct from the separate matter of what ensemble should be considered for the entire system. If one were to nondestructively follow a single realization of the system over time and assume ergodic evolution, then the correct ensemble would be the microcanonical one that has the system isolated from particle and energy exchange. This has been considered in many works [5,9,67,74,79]. On the other hand, actual experimental studies usually deal with an ensemble over many independent realizations created by cooling a new cloud each time, and independently measuring each destructively. Then the fluctuations of the number of particles between different realizations can in fact be of the same order as the mean number of particles over the whole experimental series. Due to the large number fluctuations between shots, a sequence of single clouds is likely to be more closely described by the GCE than the CE.

To wrap up this section, once correlation length scales are short enough for the LDA to be valid, the approach used here is relevant also to global properties of the system when the GCE fluctuation catastrophe is suppressed. This can happen because of any of the following: (i) lack of a true condensate; (ii) observables that do not depend on fluctuations of the condensate fraction; (iii) weak but sufficient interaction for $E_{\rm int}$ of the entire system to be large compared to the temperature; (iv) an experimental data set that consists of an ensemble of many independent realizations, except for the cases with strong post-selection on particle number. Such conditions prevail in a very wide range of systems of interest. Keeping these in mind, let us proceed.

E. Benchmarking

We will compare the classical field predictions for the observables in Sec. II C to the exact Bose gas values in the thermodynamic limit. For the ideal gas they can mostly be obtained analytically.

To proceed, the LDA approximation requires, first, the density to be correct, in the sense that an ideal gas with density n (i.e., reduced temperature τ) should be compared

to a classical field ensemble with the same density. This is also essential in practice regardless of the LDA, since n is the most basic observed quantity in experiments. To match ideal gas and classical field densities, first chemical potentials $\mu^{(\mathrm{id})}$ and $\mu^{(\mathrm{cf})}$, respectively, must be chosen. A sum over Gibbs factors gives the exact Bose gas density $n(\mu^{(\mathrm{id})})$ and the density estimate $n^{(\mathrm{cf})}(\mu^{(\mathrm{cf})}, f_c)$ in classical fields as functions of their grand canonical chemical potentials. We invert these, and with the help of Eq. (2) obtain $\mu^{(\mathrm{id})}(\tau)$ and $\mu^{(\mathrm{cf})}(\tau, f_c)$. Other observables e.g. $\varepsilon^{(\mathrm{id})}(\tau)$ and $\varepsilon^{(\mathrm{cf})}(\tau, f_c)$ can then be expressed as functions of τ and f_c as well.

In general, for the Bose ideal gas, τ and the choice of units specify all properties of the system. In classical fields, in addition to τ, the system description requires a technical parameter f_c. There, we can fit both densities $n^{(\mathrm{id})}$ and $n^{(\mathrm{cf})}$ to τ, but also we can make one other quantity agree exactly by an appropriate choice of f_c.

III. OBSERVABLE-DEPENDENT ACCURACY

A. Single observable eigencutoffs

Figure 1 shows how such cutoffs matched to different observables (which we will call eigencutoffs) behave as a function of temperature.

The density is already matched due to the LDA as explained above, and is not shown. We have also not shown results for $g^{(2)}(0)$ because it is always correctly predicted to be $g^{(2)}(0) = 2$ for every cutoff in the ideal gas. This property will not hold any more when interactions are present. Indeed, then the local density fluctuations manifest a dependence on cutoff.

The high-temperature behavior is qualitatively similar in all dimensions. The eigencutoffs matched to energy per particle f_c^{ε} and to coherence half width $f_c^{a_r}$ rise to constant values, while the eigencutoff matched for density fluctuation $f_c^{u_G}$ drops to zero (this will be commented on later in Sec. V B).

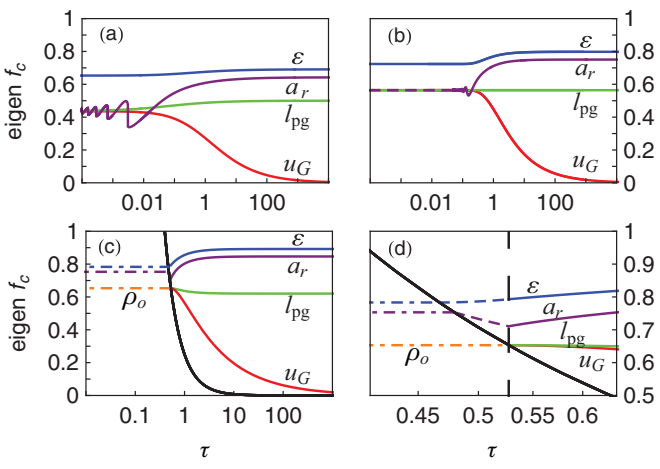

FIG. 1. (Color online) Matched eigencutoffs f_c for several observables as a function of temperature τ (ε, blue line; a_r, purple line; l_{pg}, green line; u_G, red line; ρ_o, orange line). The top panels (a), (b) show one-dimensional and two-dimensional cases, respectively, and the bottom panels present the three-dimensional situation with (d) a magnification of the critical region. The Bose gas critical temperature τ_C is marked as a vertical dashed line, while the black solid line shows the f_c value below which condensation of classical fields occurs.

The $f_c^{l_{pg}}$ takes intermediate values and is almost constant. An unexpected feature is the similar behavior of cutoffs corresponding to a_r and ε rather than the a_r and l_{pg} that are more related physically.

The crossover to low-temperature behavior is around $\tau = 1$, as expected. In the low-temperature regime, most eigencutoffs collapse to a common value (0.436 and 0.564, in 1D and 2D, respectively), except for f_c^{ε}, which prefers the higher values 0.653 and 0.724. In 3D, the cutoffs at $\tau \to 0$ are 0.783, 0.753, and 0.653 for ε, a_r, and ρ_o, respectively.

Below critical temperature in 3D, the eigencutoff for condensate fraction has a constant value. This comes about because the critical temperature in classical fields is cutoff dependent, $\tau_C^{(\mathrm{cf})} = [4 f_c]^{-2/3}$, while in the Bose gas it is $\tau_C = [\zeta(3/2)]^{-2/3} = 0.5272$ with $\zeta(3/2)$ the zeta function. The condensate fractions are directly related as $\rho_o^{(\mathrm{id})} = [1 - (\tau/\tau_C)^{\frac{3}{2}}]$ and $\rho_o^{(\mathrm{cf})} = [1 - (\tau/\tau_C^{(\mathrm{cf})})^{\frac{3}{2}}]$. Hence, $f_c^{\rho_o} = \frac{\zeta[3/2]}{4} = 0.65309$ makes $\rho_o^{(\mathrm{id})}$ and $\rho_o^{(\mathrm{cf})}$ equal for all $\tau \leqslant \tau_C$.

Two other noteworthy points are that: ($\star$) in 2D, the eigencutoff $f_c = 1/\sqrt{\pi}$ that gives the correct phase grain length l_{pg} does not depend on temperature, and ($\star\star$) the wavelike behavior of $f_c^{a_r}$ in 1D (as well as in 2D), that comes from oscillations of $g^{(1)}(\mathbf{z})$ with distance, is caused by the sharp cutoff in momentum space in classical fields.

B. Relative errors of single observables

Now, how does a nonoptimal choice of f_c affect the observables, and their systematic error? This is very relevant for practical considerations. For one thing, in a nonuniform system, when the cutoff is matched in one spatial region, it is good to know the sensitivity of results in other regions with a different density on this choice of f_c. Furthermore, we need this information to judge how good the classical fields are in describing the system overall.

The relative error δ_α of an observable α is

$$\delta_\alpha(\tau, f_c) := \frac{\Delta\alpha}{\alpha} = \left(\frac{\alpha^{(\mathrm{cf})}(\tau, f_c)}{\alpha^{(\mathrm{id})}(\tau)} - 1\right) \tag{6}$$

Its cutoff dependence is shown in Fig. 2. The first observation is that the relative error of energy per particle has an opposite trend to the other quantities. The resulting mismatch turns out to be the strongest restriction on the f_c range for which all δ_α errors are small.

Secondly, in 1D the known fact [51] that $g^{(1)}(\mathbf{z})$ and $g^{(2)}(\mathbf{z})$ do not depend on cutoffs at low τ, is reflected in small errors in l_{pg}, u_G, and a_r. However, these errors are no longer small in higher dimensions. As temperature drops, the $\delta_\alpha(\tau, f_c)$ except for δ_{ρ_o}, collapse onto curves that stay invariant with τ and remain steep (the $\tau = 0.08$ and $\tau = 0.05$ panels in Fig. 2). In other words, observables remain sensitive to cutoff all the way down to zero temperature in 2D and 3D.

IV. GLOBAL ACCURACY

What does it take to match all, or at least to be close to all typical observables? Let us consider the global error estimator

$$\mathrm{RMS}_{\alpha,\beta,\ldots}(\tau, f_c) = \sqrt{(\delta_\alpha)^2 + (\delta_\beta)^2 + \cdots}.$$

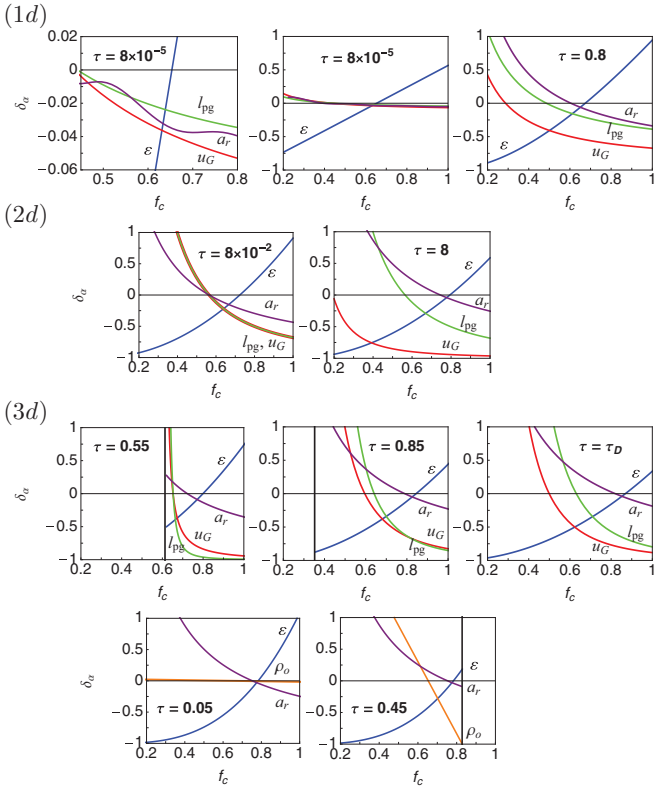

FIG. 2. (Color online) Variation of the relative errors δ_α of observables with cutoff f_c at representative high and low temperatures τ. Colors like in Fig. 1. Top row: 1D, second row: 2D, third row: 3D above τ_C, last row: 3D below τ_C.

This is a root mean square of the relative errors of chosen observables α, β, etc. Each relative error will, by definition, be less than RMS. The main aim of the function RMS will be to catch inaccuracy in any observable.

We have studied the $\mathrm{RMS}_{\alpha,\beta,\ldots}$ with all the observables that we have been considering. Moreover, we also took various combinations of them. It turns out that when we include just u_G and ε, all relevant features that were seen with larger sets of observables are covered. This happens because these quantities are the most extreme in terms of the behavior of eigen f_c and of the values and trends of δ_α. This is seen in Figs. 1 and 2. Also, the pair (ε,u_G) includes observables of second and fourth order in $\hat{\Psi}$, which are the two main classes measured in experiments. We will use them to define the quantity:

$$\mathrm{RMS}(\tau,f_c)=\sqrt{(\delta_\varepsilon)^2+(\delta_{u_G})^2} \tag{7}$$

that will be our indicator of the overall accuracy and applicability of the classical fields approximation. Below τ_C in 3D, the condensate fraction ρ_o will be used instead of u_G.

Minimizing Eq. (7) at a given temperature will give the optimal cutoff momentum and minimum error indicator minRMS. For example, a minRMS value below 0.1 (i.e., $<$10% error in observables) is often satisfactory and we will take it as a guideline.

Figure 3 shows the results for the one-dimensional gas. Global error RMS is very large above the degeneracy temperature $\tau=1$. For low temperatures it falls to zero, as one would hope. According to our 10% guideline, classical fields give acceptable results up to $\tau=0.0064$. The best choice of f_c is fairly invariant with temperature in this region, being in the range (0.649 ± 0.043). In fact, if we choose the average value of f_c, we will be close to absolute minRMS regardless of temperature or density. At high τ an extra second branch appears that is associated with a local minimum of RMS with large errors in ε and small in u_G. It is not of practical importance for us because it is less optimal.

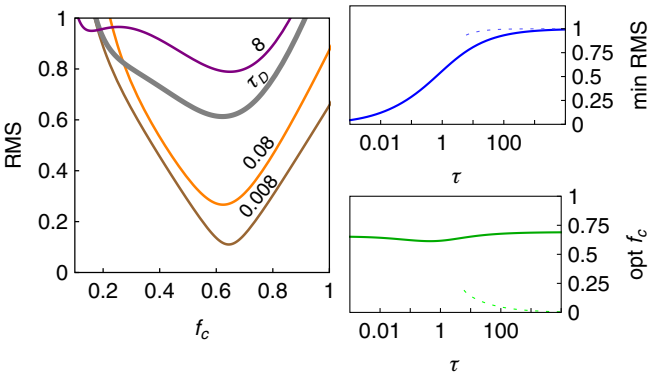

FIG. 3. (Color online) Summary results for the one-dimensional gas. The left panel shows the dependence of the global error estimator RMS, based on ε and u_G, on cutoff f_c for several values of $\tau=\{0.008$ brown, 0.08 orange, τ_D gray, 8 purple$\}$. The top right panel shows the minimal value of RMS achieved at the optimal cutoff shown in the lower right panel. An additional dashed branch indicates a less optimal local minimum of RMS.

Figure 4 shows the results for the two-dimensional gas. The behavior at low temperature is surprisingly unfavorable. RMS never falls below 0.333. This is a consequence of an inability to satisfy both observables u_G and ε. Their relative errors $\delta_{\varepsilon(u_G)}(\tau,f_c)$ become stuck on the curves shown in the fourth plot of Fig. 2 whenever $\tau\lesssim0.08$ and do not cross near zero error. One wonders whether this situation (minRMS well above 10% as $\tau\to0$) is repeated for other different sets of observables. It turns out that even the pairs (ε,l_{pg}) or (ε,a_r) will lead to similar large minRMS values. In fact, no combination that includes ε and any other observable will work

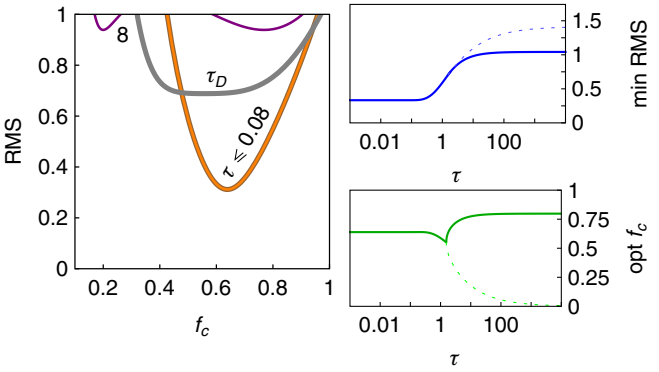

FIG. 4. (Color online) Summary results for the two-dimensional gas. Description as in Fig. 3. The $\tau=0.008$ and $\tau=0.08$ lines in the left panel overlap.

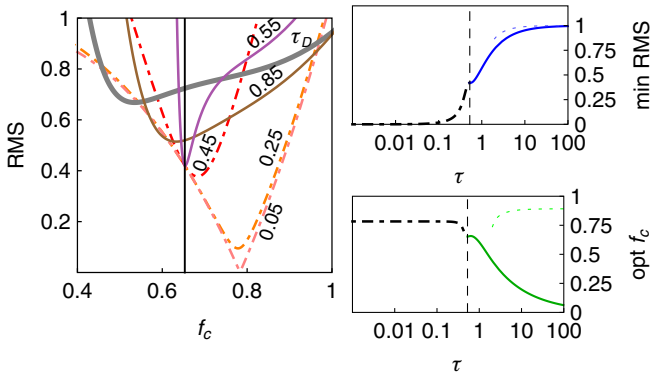

FIG. 5. (Color online) Summary results for the three-dimensional gas. The solid lines correspond to $\mathrm{RMS}_{\varepsilon,u_G}$ in the temperature region $\tau > \tau_C$ and dot-dashed lines to $\mathrm{RMS}_{\varepsilon,\rho_o}$ in the region $\tau < \tau_C$. The left panel shows the dependence of the global error estimators on cutoff f_c: $\tau = \tau_D$ gray, $\tau = 0.85$ brown, $\tau = 0.55$ purple, $\tau = 0.45$ red, $\tau = 0.25$ orange, and $\tau = 0.05$ pink. The black vertical line indicates the critical cutoff for τ_C. The right panels are as in Fig. 3, with the Bose gas critical temperature τ_C marked with a vertical dashed line and solutions below τ_C as dot-dashed lines.

well, because the $\delta_\alpha(\tau, f_c)$ curves are invariant. The crucial and *a priori* not so obvious conclusion is that in 2D, in the small temperature, ideal gas regime the classical fields description gives at best only a qualitative description of the gas, and a description that is quantitatively correct across observables is unreachable. The matter of whether this is alleviated once interactions become important warrants further study.

Figure 5 shows the results for the three-dimensional gas. The area above critical temperature behaves analogously to low dimensions. However, around the critical temperature, the RMS curve narrows and the accuracy of classical fields becomes very sensitive to the choice of the cutoff f_c. This is related to the fluctuations u_G growing to infinity at τ_C. As such, it may be related to the inequivalence of the condensed ideal gas ensembles and may be an effect that is readily removed by finite-size or interaction effects. In the condensed regime below τ_C, the RMS curve widens out again while classical fields rapidly become accurate with RMS $< 10\%$ below $\tau = 0.486\tau_C$.

V. DISCUSSION

Several points can be addressed on the basis of the ideal gas results, before considering an interacting gas.

A. Nonuniform gases

So far, we have been fully focused on the local density approach here in order to obtain results that are applicable for general inhomogeneous cloud geometries.

A very convenient aspect of what we have found is that the best cutoff value $\mathrm{opt}\, f_c$ is practically constant in the whole region where classical fields are a good description (say, minRMS $< 10\%$). This can be seen in Figs. 3 and 5, where in this region, $\mathrm{opt}\, f_c \in (0.645, 0.653)$ in 1D and $\mathrm{opt}\, f_c \in (0.778, 0.783)$ in 3D. The best low-temperature cutoff in 2D is also a constant $\mathrm{opt}\, f_c = 0.639$, see Fig. 4. Even beyond this best region, the $\mathrm{opt}\, f_c$ value is almost constant until values of $\tau \simeq 1$ are reached. For a nonuniform gas at a temperature T, the reduced temperature scales with density as $\tau(\mathbf{x}) \propto 1/[n(\mathbf{x})]^{2/d}$. Those aspects ensure that the optimum cutoff for all sections of the gas is practically the same, provided only that the bulk of the gas is quantum degenerate (i.e., $\tau(\mathbf{x}) \lesssim 1$). If it isn't, then the description is not accurate anyway. Operationally, this all means that the best cutoff to choose regardless of the density profile of the gas is

$$k_c = \frac{\mathrm{opt}\, f_c}{\hbar}\sqrt{2\pi m k_B T}; \quad \varepsilon_c = \pi(\mathrm{opt}\, f_c)^2 k_B T. \tag{8}$$

So either we take the low-temperature cutoff or it doesn't matter anyway.

The case of the uniform GCE is in fact quite well matched to the trapped canonical ensemble (CE) gas that was mentioned in Sec. II D, despite the apparently different framework of the problem. This is because the dominant central bulk of such a trapped gas is effectively a uniform open system in the LDA. The cutoffs found for the harmonically trapped canonical ensemble of the ideal gas based on condensate fraction distribution at low τ [50] correspond in our notation to values of $f_c^{(\mathrm{CE-trap})} = \{0.56, 0.72, 0.84\}$ in 1D, 2D, and 3D, respectively. These are quite close to the GCE values of $\mathrm{opt}\, f_c^{(\mathrm{LDA})} = \{0.65, 0.64, 0.78\}$ found here (Figs. 3–5). This further reinforces the view that results obtained with the LDA are also relevant for nonuniform gases, even when the entire cloud does not have particle exchange with an environment.

A certain exception is the canonical ensemble in a box whose cutoffs were also studied in Ref. [50] and found to be much lower $f_c^{(\mathrm{CE-box})} = \{0.30, 0.47, 0.65\}$. This indicates that this is a special case which describes very different physics. The matter of which ensemble should be used to describe the recently achieved box potentials [22,23,80] is still open. If the interaction is not too strong, then shot-to-shot fluctuations in energy and particle number can be appreciable and so a grand canonical approach may be warranted for the whole gas (if one is concerned with ensemble rather than time-averaged properties).

B. Breakdown mechanism at high temperatures

The reason for the drop of $f_c^{u_G}$ to zero at high τ provides an instructive example of how the classical field description breaks down. Generally the explanation comes down to different statistics of particle numbers $N_{\mathbf{k}}$ in the modes. Both the fully quantum Bose gas and the classical field have an exponentially decaying particle number distribution:

$$P(N_{\mathbf{k}}) \propto e^{(\mu - \hbar^2|\mathbf{k}|^2/2m)N_{\mathbf{k}}} \tag{9}$$

in each mode. However, in the exact treatment, $N_{\mathbf{k}}$ can only take on discrete values $0, 1, \ldots$, while in the classical fields the non-integer part of the distribution is also needed. This peculiarity very strongly increases fluctuations especially when the bulk of the distribution is in this region, i.e., the mean number of particles is $N_{\mathbf{k}} \lesssim O(1)$.

The above observations are transferred to u_G in the following way: For the exact Bose gas, the distribution is Poissonian when $N_{\mathbf{k}} \ll 1$, giving $\mathrm{var}[N_{\mathbf{k}}^{(\mathrm{id})}] = \langle N_{\mathbf{k}}^{(\mathrm{id})} \rangle$ for each

mode, while the exponential distribution in classical fields gives $\mathrm{var}[N_{\mathbf{k}}^{(\mathrm{cf})}] = \langle N_{\mathbf{k}}^{(\mathrm{cf})}\rangle^2$. Due to having independent modes, $u_G = \sum_{\mathbf{k}} \mathrm{var}[N_{\mathbf{k}}] \; / \sum_{\mathbf{k}} \langle N_{\mathbf{k}}\rangle$, and in the exact treatment $u_G \to 1$ directly. To obtain the same with classical fields, occupations $N_{\mathbf{k}}^{(\mathrm{cf})} \sim 1$ are necessary to make $\mathrm{var}[N_{\mathbf{k}}] \approx \langle N_{\mathbf{k}}\rangle$. These are much greater than in the Bose gas. So to also simultaneously match overall density of the many-mode gas, the cutoff must be made much lower than the Bose gas momentum width $2\pi/\Lambda_T$ so as to get the same area under the distribution of density in k space. From (3), this immediately implies $f_c^{u_G} \ll 1$. With such a great modification of $N(\mathbf{k})$, correctly matching additional observables like ε with classical fields becomes out of the question.

A similar breakdown can be expected whenever the physics is captured by low-occupied independent modes. For example, such discrepancies were seen between experiment and classical fields in the quantum Bogoliubov regime of the interacting gas at very low temperatures [65].

VI. CROSSOVER TO THE INTERACTING GAS

An obvious question is whether the ideal gas results carry over into the interacting gas. To address this, we have benchmarked the classical field description in one-dimensional systems with the Yang-Yang exact solution for the uniform interacting Bose gas [64] for a sequence of increasing interaction strengths that cover the crossover from the ideal gas to an interaction-induced quasicondensate.

A. Procedure

The exact values for $n = N/L$, as well as system energy E in a segment of length L can be obtained via the self-consistent numerical solution of the integral equations given in the original Yang-Yang paper [64]. The Hellmann-Feynman theorem was used by Kheruntsyan *et al.* to obtain $g^{(2)}(0) = -\frac{1}{n^2}(\partial P/\partial g)_{\mu,T}$ from the Yang-Yang solution for pressure P [81,82], which can be readily evaluated numerically. For the contact-interacting gas the expression for the interaction energy in the system is $E_{\mathrm{int}} = \frac{1}{2}gn^2Lg^{(2)}(0)$. From this, one obtains the kinetic energy per particle: $\varepsilon_{\mathrm{kin}} = (E - E_{\mathrm{int}})/N$. The coarse-grained density fluctuations can also be found via $u_G = \frac{k_BT}{n}(\partial n/\partial\mu)_T$, based on the expression for $\mathrm{var}[N]$ in Ref. [66].

To obtain classical field results, we generate ensembles of classical field realizations $\Psi(x)$ using a Metropolis algorithm, in a way conceptually similar to the work of Witkowska *et al.* [55] but using grand canonical ensemble weights $e^{[\mu N(\Psi)-E(\Psi)]/k_BT}$. The numerical lattice is chosen to have a box of length L with periodic boundary conditions that is wide enough for the density and phase correlations to decay to zero before wrapping around. The number of points was 2^{10}, which is easily sufficient for the maximum numerical lattice wave vector to be many times larger than the cutoffs k_c imposed on the field in k space. This ensures that no aliasing problems appear for the evaluation of the interaction energy term, as has been discussed in the context of the padded lattice in the PGPE and truncated Wigner methods [83]. Classical field values for observables at a given cutoff are calculated using 10^4 ensemble members.

For each cutoff, the observables are benchmarked against exact Yang-Yang values for systems having the same values of T, g, and density n as the classical field ensemble. It remains true for the interacting gas that u_G and $\varepsilon_{\mathrm{kin}}$ have the most extreme behavior among the set of observables that now also include the interaction energy per particle and $g^{(2)}(0)$. The latter two have a cutoff-dependent behavior that is somewhat similar to u_G. Hence, we continue to use the same global accuracy indicator (7) as for the ideal gas, using the kinetic energy per particle $\varepsilon_{\mathrm{kin}}$ and coarse-grained fluctuations u_G. minRMS and opt f_c are obtained by fitting a function to the cutoff-dependent values of $\mathrm{RMS}(\tau, f_c)$ at a given τ and γ. We use the square root of a parabola because it is a good candidate for describing the f_c-dependent behavior of $\mathrm{RMS}(\tau, f_c)$ near the minimum. It marries the approximately linear behavior of δ_ε and δ_{u_G} in this region that is seen in Fig. 2, with the expression (7) for RMS. We use data from an f_c range of about ± 0.05 around the minimum. Error bars are obtained by splitting the field samples into N_S smaller subensembles, calculating subensemble values of $\mathrm{minRMS}^{(i)}$ and $\mathrm{opt}\, f_c^{(i)}$ in the same way for each, and invoking

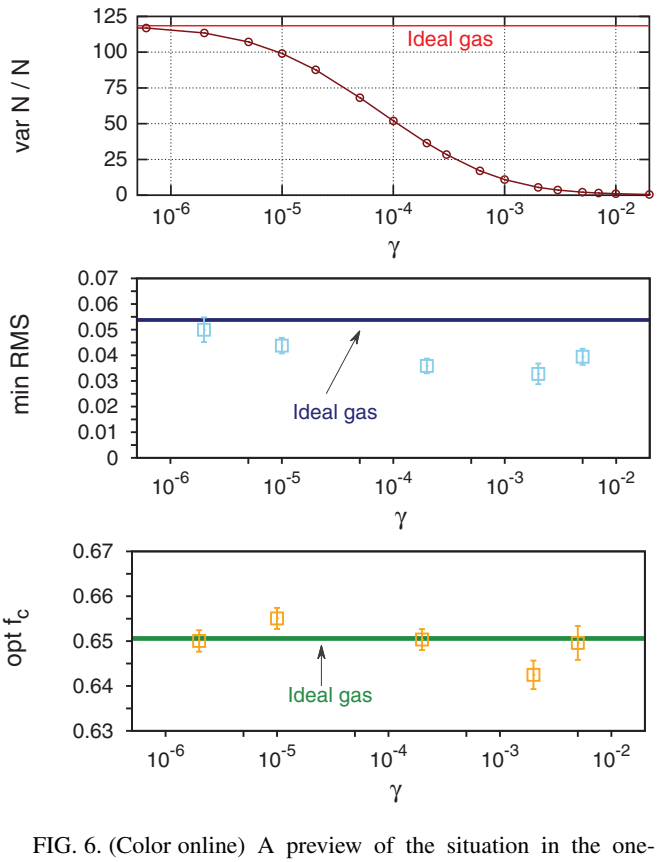

FIG. 6. (Color online) A preview of the situation in the one-dimensional interacting gas. Here, $\tau = 0.00159$, and $\gamma = g/n$ increases to the right. Top: the change in u_G, obtained from the Yang-Yang [64] exact solution, compared to the ideal gas $\gamma \to 0$ value (red). Middle: minimal value of RMS as in Figs. 3–5 with 1σ statistical error bars from an ensemble of 10^4 samples, and the ideal gas value shown as the horizontal line. Bottom: corresponding optimum cutoff f_c and its ideal gas value. One sees that while the observable u_G changes by two orders of magnitude, the ideal gas values for cutoff and accuracy carry over onto the interacting gas.

the central limit theorem to estimate the uncertainty in the full-ensemble values to be $\Delta\mathrm{opt}\, f_c = \sqrt{\mathrm{var}[\mathrm{opt}\, f_c^{(i)}]/N_S}$ and $\Delta\mathrm{minRMS} = \sqrt{\mathrm{var}[\mathrm{minRMS}^{(i)}]/N_S}$.

B. Results

We have carried out the above benchmarking for the reduced temperature $\tau = 0.00159$ and a range of interaction strengths $\gamma = g/n$ from 2×10^{-6} to 0.005 in the dilute interacting gas. These are experimentally realistic parameters. The local bunching $g^{(2)}(0)$ changes over this range from 1.976 in the very weakly interacting limit to 1.02 at $\gamma = 0.005$. This indicates that we move from an almost perfect ideal gas on the left deep into the strong quasicondensate regime on the right, where almost all effects are dominated by the interaction mean field. The coarse-grained density fluctuations change by two orders of magnitude over this range, as plotted in the top panel of Fig. 6.

The results of this foray into the interacting gas are shown in the other panels of Fig. 6. The ideal gas values for cutoff carry over onto the interacting gas unchanged, to within available statistical precision. The global accuracy minRMS actually improves. One concludes then that in this regime at least the optimum cutoff and degree of accuracy found in the ideal gas applies very well to a wide swath of the interacting gas as well. This is not an *a priori* obvious result, but certainly a convenient and encouraging one for those who want to make calculations using classical fields.

VII. CONCLUSIONS

To conclude, we have judged the goodness of classical fields for describing the ideal Bose gas in 1D, 2D, and 3D using all the usually measured observables. We have shown that 10% or better accuracy for the whole set of observables simultaneously is possible in 1D up to temperatures of $T = 0.0064 T_d$ with the cutoff prescription $k_c \approx 0.65(\frac{2\pi}{\Lambda_T})$ and in 3D up to $T = 0.49 T_c$ with $k_c \approx 0.78\,(\frac{2\pi}{\Lambda_T})$. The essence of the matter can be captured by the indicator RMS based on kinetic energy per particle and coarse-grained density fluctuations, which are the observables that are the hardest to mutually satisfy.

In 2D, we have found a surprising feature that classical fields remain incapable of properly describing all the observables together in the ideal gas even as $T \to 0$. One suspects that finite size effects and/or weak interactions may improve agreement here. The indication is that something is going on in 2D that warrants further study.

When a system is correctly described with a classical ensemble of complex fields as here, the observation of many intrinsically quantum effects that rely on wave-particle duality or a discretization of the basis is ruled out. This includes things such as stronger-than-classical correlations, Heisenberg uncertainty relations, mode entanglement, EPR and Bell inequality violation, antibunching, and noncommuting observables. All in line with the difference between classical optics on the one hand and quantum optics and quantum information theory on the other. Thus, for parameters in which the weakly interacting Bose gas is described by the classical field to some level of RMS, observation of the above intrinsically quantum effects with typical observables will also be suppressed to a level of the same order as RMS. Of course, large RMS is not sufficient to imply quantum effects.

Two results lead to optimistic conclusions for the practical application of classical fields to ultracold gases. First, the optimum cutoffs in the ideal gas are almost unchanged with τ in the whole region where accuracy is good. This means that even for a nonuniform cloud with a common global temperature, a single cutoff value is close to optimal in the entire degenerate region. This goes a long way towards pacifying one of the leading practical worries. Second, our study of the crossover into the interacting gas in Sec. VI shows that the cutoff that optimizes the ideal gas is also valid for a part of the interacting gas, including a region where the quasicondensate is dominated by interactions. The degree of accuracy seen in the ideal gas is also preserved. This is a nontrivial but very encouraging result. A more detailed study of the situation for the whole range of interaction strengths in 1D is a subject for future research.

ACKNOWLEDGMENTS

We would like to address our thanks to Vyacheslav I. Yukalov and Matthew Davis for their attention and comments to us on this matter. This work was supported by the National Science Centre (Poland) Grant No. 2012/07/E/ST2/01389.

[1] M. Brewczyk, M. Gajda, and K. Rzążewski, J. Phys. B **40**, R1 (2007).
[2] N. P. Proukakis and B. Jackson, J. Phys. B **41**, 203002 (2008).
[3] P. B. Blakie, A. S. Bradley, M. J. Davis, R. J. Ballagh, and C. W. Gardiner, Adv. Phys. **57**, 363 (2008).
[4] *Quantum Gases: Finite Temperature and Non-Equilibrium Dynamics*, edited by N. Proukakis, S. Gardiner, M. Davis, and M. Szymańska, Vol. 1 Cold Atoms Series (World Scientific, Singapore, 2013).
[5] Y. Kagan and B. V. Svistunov, Phys. Rev. Lett. **79**, 3331 (1997).
[6] M. J. Davis, S. A. Morgan, and K. Burnett, Phys. Rev. Lett. **87**, 160402 (2001).
[7] K. Góral, M. Gajda, and K. Rzążewski, Opt. Express **8**, 92 (2001).
[8] N. G. Berloff and B. V. Svistunov, Phys. Rev. A **66**, 013603 (2002).
[9] H. T. C. Stoof, J. Low Temp. Phys. **114**, 11 (1999).
[10] C. W. Gardiner and M. J. Davis, J. Phys. B **36**, 4731 (2003).
[11] M. J. Steel, M. K. Olsen, L. I. Plimak, P. D. Drummond, S. M. Tan, M. J. Collett, D. F. Walls, and R. Graham, Phys. Rev. A **58**, 4824 (1998).
[12] A. Sinatra, C. Lobo, and Y. Castin, J. Phys. B **35**, 3599 (2002).
[13] A. Polkovnikov, Ann. Phys. (N.Y.) **325**, 1790 (2010).
[14] M. Wouters and V. Savona, Phys. Rev. B **79**, 165302 (2009).
[15] A. Chiocchetta and I. Carusotto, Phys. Rev. A **90**, 023633 (2014).
[16] S. Ayik, Phys. Lett. B **658**, 174 (2008).
[17] D. Lacroix, D. Gambacurta, and S. Ayik, Phys. Rev. C **87**, 061302(R) (2013).

[18] S. N. Klimin, J. Tempere, G. Lombardi, and J. T. Devreese, Eur. Phys. J. B **88**, 122 (2015).
[19] S. Simonucci and G. C. Strinati, Phys. Rev. B **89**, 054511 (2014).
[20] M. Gring, M. Kuhnert, T. Langen, T. Kitagawa, B. Rauer, M. Schreitl, I. Mazets, D. Adu Smith, E. Demler, and J. Schmiedmayer, Science **337**, 1318 (2012).
[21] T. Langen, M. Gring, M. Kuhnert, B. Rauer, R. Geiger, D. Adu Smith, I. E. Mazets, and J. Schmiedmayer, Eur. Phys. J. Special Topics **217**, 43 (2013).
[22] L. Chomaz, L. Corman, T. Bienaimé, R. Desbuquois, C. Weitenberg, S. Nascimbéne, J. Beugnon, and J. Dalibard, Nat. Commun. **6**, 6162 (2015).
[23] N. Navon, A. L. Gaunt, R. P. Smith, and Z. Hadzibabic, Science **347**, 167 (2015).
[24] S. Serafini, M. Barbiero, M. Debortoli, S. Donadello, F. Larcher, F. Dalfovo, G. Lamporesi, and G. Ferrari, Phys. Rev. Lett. **115**, 170402 (2015).
[25] G. Lamporesi, S. Donadello, S. Serafini, F. Dalfovo, and G. Ferrari, Nat. Phys. **9**, 656 (2013).
[26] S. Donadello, S. Serafini, M. Tylutki, L. P. Pitaevskii, F. Dalfovo, G. Lamporesi, and G. Ferrari, Phys. Rev. Lett. **113**, 065302 (2014).
[27] L. E. Sadler, J. M. Higbie, S. R. Leslie, M. Vengalattore, and D. M. Stamper-Kurn, Nature (London) **443**, 312 (2006).
[28] C. N. Weiler, T. W. Neely, D. R. Scherer, A. S. Bradley, M. J. Davis, and B. P. Anderson, Nature **455**, 948 (2008).
[29] C. V. Parker, L.-C. Ha, and C. Chin, Nat. Phys. **9**, 769 (2013).
[30] T. Karpiuk, P. Deuar, P. Bienias, E. Witkowska, K. Pawłowski, M. Gajda, K. Rzążewski, and M. Brewczyk, Phys. Rev. Lett. **109**, 205302 (2012).
[31] B. Nowak, D. Sexty, and T. Gasenzer, Phys. Rev. B **84**, 020506(R) (2011).
[32] M. Schmidt, S. Erne, B. Nowak, D. Sexty, and T. Gasenzer, New J. Phys. **14**, 075005 (2012).
[33] J. Sabbatini, W. H. Żurek, and M. J. Davis, New J. Phys. **14**, 095030 (2012).
[34] T. Simula, M. J. Davis, and K. Helmerson, Phys. Rev. Lett. **113**, 165302 (2014).
[35] S. P. Cockburn, H. E. Nistazakis, T. P. Horikis, P. G. Kevrekidis, N. P. Proukakis, and D. J. Frantzeskakis, Phys. Rev. A **84**, 043640 (2011).
[36] I.-K. Liu, R. W. Pattinson, T. P. Billam, S. A. Gardiner, S. L. Cornish, T.-M. Huang, W.-W. Lin, S.-C. Gou, N. G. Parker, and N. P. Proukakis, arXiv:1408.0891.
[37] E. Witkowska, T. Świsłocki, and M. Matuszewski, Phys. Rev. A **90**, 033604 (2014).
[38] E. Witkowska, J. Dziarmaga, T. Świsłocki, and M. Matuszewski, Phys. Rev. B **88**, 054508 (2013).
[39] T. Świsłocki, E. Witkowska, J. Dziarmaga, and M. Matuszewski, Phys. Rev. Lett. **110**, 045303 (2013).
[40] E. Witkowska, P. Deuar, M. Gajda, and K. Rzążewski, Phys. Rev. Lett. **106**, 135301 (2011).
[41] R. N. Bisset, M. J. Davis, T. P. Simula, and P. B. Blakie, Phys. Rev. A **79**, 033626 (2009).
[42] A. D. Martin and J. Ruostekoski, Phys. Rev. Lett. **104**, 194102 (2010).
[43] A. D. Martin and J. Ruostekoski, New J. Phys. **12**, 055018 (2010).
[44] R. Barnett, A. Polkovnikov, and M. Vengalattore, Phys. Rev. A **84**, 023606 (2011).
[45] S. Dettmer, D. Hellweg, P. Ryytty, J. J. Arlt, W. Ertmer, K. Sengstock, D. S. Petrov, G. V. Shlyapnikov, H. Kreutzmann, L. Santos, and M. Lewenstein, Phys. Rev. Lett. **87**, 160406 (2001).
[46] M. J. Davis, S. A. Morgan, and K. Burnett, Phys. Rev. A **66**, 053618 (2002).
[47] A. S. Bradley, P. B. Blakie, and C. W. Gardiner, J. Phys. B **38**, 4259 (2005).
[48] S. P. Cockburn, A. Negretti, N. P. Proukakis, and C. Henkel, Phys. Rev. A **83**, 043619 (2011).
[49] T. Karpiuk, M. Brewczyk, M. Gajda, and K. Rzążewski, Phys. Rev. A **81**, 013629 (2010).
[50] E. Witkowska, M. Gajda, and K. Rzążewski, Phys. Rev. A **79**, 033631 (2009).
[51] Y. Castin, J. Phys. IV (France) **116**, 89 (2004).
[52] M. J. Davis and S. A. Morgan, Phys. Rev. A **68**, 053615 (2003).
[53] M. Brewczyk, P. Borowski, M. Gajda, and K. Rzążewski, J. Phys. B **37**, 2725 (2004).
[54] L. Zawitkowski, M. Brewczyk, M. Gajda, and K. Rzążewski, Phys. Rev. A **70**, 033614 (2004).
[55] E. Witkowska, M. Gajda, and K. Rzążewski, Opt. Commun. **283**, 671 (2010).
[56] T. M. Wright, N. P. Proukakis, and M. J. Davis, Phys. Rev. A **84**, 023608 (2011).
[57] P. Bienias, K. Pawłowski, M. Gajda, and K. Rzążewski, Phys. Rev. A **83**, 033610 (2011).
[58] P. Bienias, K. Pawłowski, M. Gajda, and K. Rzążewski, Europhys. Lett. **96**, 10011 (2011).
[59] P. B. Blakie, Phys. Rev. E **78**, 026704 (2008).
[60] S. P. Cockburn, D. Gallucci, and N. P. Proukakis, Phys. Rev. A **84**, 023613 (2011).
[61] D. Gallucci, S. P. Cockburn, and N. P. Proukakis, Phys. Rev. A **86**, 013627 (2012).
[62] S. P. Cockburn and N. P. Proukakis, Phys. Rev. A **86**, 033610 (2012).
[63] M. Lewin, P. T. Nam, and N. Rougerie, arXiv:1410.0335.
[64] C. N. Yang and C. P. Yang, J. Math. Phys. **10**, 1115 (1969).
[65] J. Armijo, Phys. Rev. Lett. **108**, 225306 (2012).
[66] J. Armijo, T. Jacqmin, K. V. Kheruntsyan, and I. Bouchoule, Phys. Rev. A **83**, 021605(R) (2011).
[67] M. Gajda and K. Rzążewski, Phys. Rev. Lett. **78**, 2686 (1997).
[68] S. Grossmann and M. Holthaus, Phys. Rev. E **54**, 3495 (1996).
[69] S. Grossmann and M. Holthaus, Opt. Express **1**, 262 (1997).
[70] C. Weiss and M. Wilkens, Opt. Express **1**, 272 (1997).
[71] H. D. Politzer, Phys. Rev. A **54**, 5048 (1996).
[72] S. Giorgini, L. P. Pitaevskii, and S. Stringari, Phys. Rev. Lett. **80**, 5040 (1998).
[73] Z. Idziaszek, M. Gajda, P. Navez, M. Wilkens, and K. Rzążewski, Phys. Rev. Lett. **82**, 4376 (1999).
[74] P. Navez, D. Bitouk, M. Gajda, Z. Idziaszek, and K. Rzążewski, Phys. Rev. Lett. **79**, 1789 (1997).
[75] V. I. Yukalov, Phys. Lett. A **340**, 369 (2005).
[76] V. I. Yukalov, Las. Phys. Lett. **6**, 688 (2009).
[77] V. I. Yukalov, Phys. Part. Nuclei **42**, 460 (2011).

[78] V. V. Kocharovsky, V. V. Kocharovsky, M. Holthaus, C. H. R. Ooi, A. Svidzinsky, W. Ketterle, and M. O. Scully, Adv. At. Mol. Opt. Phys. **53**, 291 (2006).

[79] K. Góral, M. Gajda, and K. Rzążewski, Phys. Rev. A **66**, 051602(R) (2002).

[80] I. Gotlibovych, T. F. Schmidutz, A. L. Gaunt, N. Navon, R. P. Smith, and Z. Hadzibabic, Phys. Rev. A **89**, 061604(R) (2014).

[81] K. V. Kheruntsyan, D. M. Gangardt, P. D. Drummond, and G. V. Shlyapnikov, Phys. Rev. Lett. **91**, 040403 (2003).

[82] K. V. Kheruntsyan, D. M. Gangardt, P. D. Drummond, and G. V. Shlyapnikov, Phys. Rev. A **71**, 053615 (2005).

[83] A. A. Norrie, R. J. Ballagh, and C. W. Gardiner, Phys. Rev. A **73**, 043617 (2006).